Nomination form for the 2021 Nishina Asia Award

Candidate (name, affiliation, curriculum vitae including the date of the degree of Ph.D., nationality, address, email and telephone)
Name: Ying Zhang Affiliation: Department of Physics, School of Science, Tianjin University, Tianjin, China Nationality: Chinese Address: Room 327, Building 32, Beiyang Campus, Tianjin University, No. 135 Yaguan Road, Jinnan, 300354, Tianjin, China Email: Telephone: +86-189-2081-2593 Curriculum vitae: 2019. 10 – 2020. 10, Visiting Researcher, RIKEN (Wako), China 2016. 1– now, Associate Professor, Tianjin University, Tianjin, China. 2013. 9 – 2015.12, Assistant Professor, Tianjin University, Tianjin, China. 2012.9 – 2013.8, Assistant Professor, Niigata University, Japan 2012.2 – 2012.8, Postdoctoral Researcher, Peking University, China 2011.4 – 2012.1, Postdoctoral Researcher, RIKEN (Wako), Japan 2011.1 – 2011.3, Postdoctoral Researcher, Peking University, China 2011. 1. 5, Ph.D, Major: Theoretical Particle and Nuclear Physics, School of Physics, Peking University, Beijing, China. Supervisor: Jie Meng 2005. 6, B.Sc, Major: Physics, School of Physics, Nankai University, Tianjin, China
Citation for the Award (within 30 words)
Her contributions to develop the innovative techniques in the density functional theory to achieve the microscopic and self-consistent description of the neutron-rich nucleus.

Description of the work

The worldwide construction of large-scale nuclear facilities provided us a lot of new information about neutron/proton-rich nuclei. This new information is very helpful to examine and improve the present nuclear theory models. In neutron-rich nuclei, since the valence neutrons are weakly bound, their spatial density distributions are very extended. Therefore, theoretically one needs to deal with the continuum effect properly in the coordinate space. The candidate has been working within the density functional theory, and innovatively introduced the Green's function method to the Skyrme Hartree-Fock-Bogoliubov (HFB) model. Taking the advantage of the description of the continuum states, the Green's function can help to provide nicely the extended density distribution of neutron-rich nuclei. At the same time, the contribution from the resonant states in the continuum can be included self-consistently to the bulk properties of the neutron-rich nuclei.

With this new method, the candidate investigated the role of the weakly bound and resonant states in N=86 isotones in the pairing correlation [1]. According to a simple imagination, these states may decouple from the pairing correlation due to their extended wave functions. However, the candidate found they persist to feel and contribute to the pairing correlation, due to the self-consistency. The candidate also applied this new method to investigate the giant halo phenomenon predicted in neutron-rich Zr isotopes [2]. There, she found the asymptotic behavior of the pair density is determined by the low-lying non resonant continuum states, different from that of the particle density which is determined by the low-lying resonant states. Besides, the candidate successfully introduced the imaginary time step method which is very flexible to describe the deformed nuclei in the coordinate space to the relativistic mean-field model [3]. The candidate innovatively overcame the "disaster of the tsunami" when applying this method in the relativistic theory, and inspired a lot of other works similar to this idea for the description of the deformed neutron-rich nuclei in the coordinate space.

Key references (up to 3 key publications*)

[1].
"Persistent contribution of unbound states to the pair correlation in continuum Skyrme-Hartree-Fock-Bogoliubov approach",
Ying Zhang, Masayuki Matsuo, Jie Meng*, Physical Review C 83, 054301 (2011)

[2]. "Pair correlation of giant halo nuclei in continuum Skyrme-Hartree-Fock-Bogoliubov theory",
Ying Zhang*, Masayuki Matsuo, Jie Meng, Physical Review C 86, 054318 (2012)

[3]. "Avoid the Tsunami of the Dirac sea in the Imaginary Time Step method"
Ying Zhang*, Haozhao Liang, and Jie Meng,
International Journal of Modern Physics E, Vol. 19, No. 1, 55-62 (2010).

*) Copy of one most significant publication should be attached.

Nominator (name, affiliation, email, telephone and relation to the candidate)
Name: Hideo Ohno Affiliation: President, Tohoku University, Japan Nationality: Japan Address: 2-1-1 Katahira, Aoba-ku, Sendai, Miyagi 980-8577 Japan Email: kenkyo-kikaku@grp.tohoku.ac.jp Telephone: +81-22-217-5014
Signature Hideo Ohno Date March 31, 2021

PHYSICAL REVIEW C **83**, 054301 (2011)

Persistent contribution of unbound quasiparticles to the pair correlation in the continuum Skyrme-Hartree-Fock-Bogoliubov approach

Y. Zhang (张颖),[1,2] M. Matsuo (松尾正之),[2,3,4] and J. Meng (孟杰)[4,1,5,*]
[1] *State Key Laboratory of Nuclear Physics and Technology, School of Physics, Peking University, Beijing 100871, China*
[2] *Graduate School of Science and Technology, Niigata University, Niigata 950-2181, Japan*
[3] *Department of Physics, Faculty of Science, Niigata University, Niigata 950-2181, Japan*
[4] *School of Physics and Nuclear Energy Engineering, Beihang University, Beijing 100191, China*
[5] *Department of Physics, University of Stellenbosch, Stellenbosch, South Africa*
(Received 14 December 2010; revised manuscript received 24 February 2011; published 3 May 2011)

The neutron pair correlation in nuclei near the neutron drip-line is investigated using the self-consistent continuum Skyrme-Hartree-Fock-Bogoliubov theory formulated with the coordinate-space Green's function technique. Numerical analysis is performed for even-even $N = 86$ isotones in the Mo-Sn region, where the $3p_{3/2}$ and $3p_{1/2}$ orbits lying near the Fermi energy are either weakly bound or unbound. The quasiparticle states originating from the $l = 1$ orbits form resonances with large widths, which are due to the low barrier height and the strong continuum coupling caused by the pair potential. Analyzing in detail the pairing properties and roles of the quasiparticle resonances, we found that the $l = 1$ broad quasiparticle resonances persist to feel the pair potential and contribute to the pair correlation even when their widths are comparable with the resonance energy.

DOI: 10.1103/PhysRevC.83.054301 PACS number(s): 21.10.Gv, 21.10.Pc, 21.60.Jz, 27.60.+j

I. INTRODUCTION

Recently, interest has been focused on pairing properties of neutron-rich nuclei near the drip-line. The most peculiar case could be the firstly observed halo nucleus, ^{11}Li, where two neutrons forming the halo would not be bound to the nucleus if the pair correlation was absent [1–4]. Similar examples are also suggested in nuclei near the neutron drip-line in heavier mass regions, e.g., possible giant halo structure (consisting of more than two neutrons) which is predicted in Ca and Zr isotopes by the self-consistent mean-field models [5–10]. A new aspect in these examples is that the pair correlation occurs among neutrons occupying unbound or weakly bound orbits with low angular momentum $l = 0$ or 1 whose wave functions extend far outside the nucleus due to the low (zero) centrifugal barrier.

A useful theoretical tool to study the pair correlation in the weakly bound nuclei in all the mass regions, except the lightest ones, is the coordinate-space Hartree-Fock-Bogoliubov (HFB) approach [11–14], in which the quasiparticle wave functions of weakly bound and unbound nucleons are described in the coordinate-space representation. Indeed the pairing properties in nuclei near the drip-line have been studied extensively within the HFB scheme [8,15–25] as well as the relativistic Hartree(-Fock)-Bogoliubov models [4–6,14,26–29]. The pair correlation we deal with here is, however, a rather complex and unresolved problem, and there exist controversial issues concerning the roles of weakly bound and unbound orbits. For instance, it has been argued in Refs. [21–24] that neutrons in the weakly bound and unbound orbits with $l = 0$ and 1 tend to decouple from the pair field generated by the other neutrons because of the large spatial extension of their wave functions. It is also claimed that those neutrons contribute very little to the total pair correlation in nuclei. On the contrary, other studies show large pairing effects even on the weakly bound neutrons, leading to the pairing antihalo effect [30] and the increase of the neutron pairing gap for weaker binding of neutrons or for shallower neutron Fermi energy [17,18].

In this paper, we would like to present an investigation of the pairing properties of nuclei close to the neutron drip-line, with intentions to clarify the roles of weakly bound and unbound orbits with low angular momenta.

To perform this study, there exist some physically and technically important points which need to be treated carefully. Firstly, precise description of the wave functions outside the nucleus must be guaranteed since we deal with weakly bound and unbound orbits. We achieve it in the present study by using the coordinate-space mesh representation for the Skyrme-Hartree-Fock-Bogoliubov model [12].

Secondly, also related to the first point, a suitable boundary condition needs to be imposed on the wave functions of the quasiparticle states in the continuum, which also have a sizable contribution to the pair correlation in the case of nuclei with a shallow Fermi energy close to zero. Note here that the quasiparticle states whose excitation energy exceeds the separation energy form the continuum spectrum because they couple to scattering waves [11–13]. The Hartree-Fock single-particle orbits emerge as resonant quasiparticle states with finite width [13]. To describe this situation, one needs to guarantee the asymptotic form of the quasiparticle wave function as the scattering wave. In this way, we can avoid artificial discretization of the continuum spectrum, and can evaluate the width of a resonant quasiparticle state. This allows us to investigate how the resonant quasiparticle states contribute to the pair correlation.

Thirdly, it is important to describe self-consistently the pair potential, which is the key quantity describing the pair correlation. To achieve this, however, the continuum quasiparticle states, including both resonant and nonresonant states, are to be summed up in evaluating the one-body

*mengj@pku.edu.cn

densities. We adopt the Green's function technique [13] that provides a simple and effective way of summing. Thus, we are able to perform in the present work the fully self-consistent continuum Hartree-Fock-Bogoliubov calculations, i.e., we derive self-consistently both the Hartree-Fock potential (using the Skyrme functional) and the pair potential (using a density-dependent contact interaction as the effective pairing force). The theoretical framework of the present analysis shares many common aspects with those in Refs. [21–24], but we utilize the self-consistent pair potential as well as the Hartree-Fock mean field. Compared with the continuum Skyrme-HFB calculations formulated in Refs. [8,16], we utilize the scattering wave functions to construct the Green's function. A similar continuum HFB calculation with Green's function technique has been performed in Ref. [25] but with DF3 density functional of finite Fermi system theory and contact gradient pairing force.

We will perform numerical analysis for the $N = 86$ isotones in the Mo-Sn region. The Skyrme-HFB theory with the parameter set SLy4 suggests the presence of weakly bound neutron single-particle orbits above the $N = 82$ shell gap in neutron rich nuclei with $N \gtrsim 84$ and $Z \lesssim 50$. In the $N = 86$ isotones, particularly, the $3p_{1/2}$ and $3p_{3/2}$ orbits emerge close to the zero energy with the Hartree-Fock single-particle energies ranging from $\varepsilon \sim -0.5$ MeV to unbound resonances around $\varepsilon \sim 0.7$ MeV. Hence it provides us with a good testing ground to study the role of weakly bound low-l orbits in the pair correlation.

In the numerical analysis, we shall pay special attentions to the pair density (called also the pairing tensor or the abnormal density in the literature) and the related quantities. The pair density is one of the most relevant quantities to the pair correlation since it shows up in the definitions of both the self-consistent pair potential and the pair correlation energy. Using this quantity we will show that the $l = 1$ weakly bound or unbound orbits keep a finite and sizable contribution to the pair correlation even when they form very broad quasiparticle resonances, and when they are located above the potential barrier. The pairing gap associated with the unbound quasiparticle states are also found to stay finite. This result is different from those in Refs. [21–24], which suggest the decoupling of the $l = 0, 1$ weakly bound and unbound orbits from the pair correlation. We shall discuss the origin of the difference.

Finally, we remark that the present analysis is related to Ref. [18], where, however, the Hartree-Fock potential is replaced by a simple Woods-Saxon potential although the deformation effect is taken into account. In the present work, we do not discuss the deformation effect for simplicity, but instead we investigate in detail the roles of weakly bound and unbound orbits especially with the low angular momentum by using the fully self-consistent continuum Hartree-Fock-Bogoliubov calculations assuming the spherical symmetry.

In Sec. II, we describe the formulation of the continuum Skyrme-HFB theory using the Green's function technique. After presenting the results including the numerical details and the related discussions in Sec. III, we draw conclusions in Sec. IV.

II. FORMALISM

A. Hartree-Fock-Bogoliubov equation with Skyrme interaction

In the Hartree-Fock-Bogoliubov (HFB) theory, the pair-correlated nuclear system is described in terms of the independent quasiparticles. The HFB equation for the quasiparticle wave function $\phi_i(\mathbf{r}\sigma)$ in the coordinate space is

$$\int d\boldsymbol{r}' \sum_{\sigma'} \begin{pmatrix} h(\boldsymbol{r}\sigma, \boldsymbol{r}'\sigma') - \lambda\delta(\boldsymbol{r}-\boldsymbol{r}')\delta_{\sigma\sigma'} & \tilde{h}(\boldsymbol{r}\sigma, \boldsymbol{r}'\sigma') \\ \tilde{h}^*(\boldsymbol{r}\tilde{\sigma}, \boldsymbol{r}'\tilde{\sigma}') & -h^*(\boldsymbol{r}\tilde{\sigma}, \boldsymbol{r}'\tilde{\sigma}') + \lambda\delta(\boldsymbol{r}-\boldsymbol{r}')\delta_{\sigma\sigma'} \end{pmatrix} \phi_i(\boldsymbol{r}'\sigma') = E_i\phi_i(\boldsymbol{r}\sigma), \tag{1}$$

where E_i is the quasiparticle energy, and λ is the chemical potential or the Fermi energy. The Hartree-Fock Hamiltonian h and the pair Hamiltonian $\tilde{h}$ can be obtained by the variation of the total energy functional with respect to the particle density matrix $\rho(\boldsymbol{r}\sigma, \boldsymbol{r}'\sigma')$ and pair density matrix $\tilde{\rho}(\boldsymbol{r}\sigma, \boldsymbol{r}'\sigma')$, respectively. The two density matrices can be combined in a generalized density matrix $\mathcal{R}$ as

$$\mathcal{R}(\boldsymbol{r}\sigma, \boldsymbol{r}'\sigma') \equiv \begin{pmatrix} \rho(\boldsymbol{r}\sigma, \boldsymbol{r}'\sigma') & \tilde{\rho}(\boldsymbol{r}\sigma, \boldsymbol{r}'\sigma') \\ \tilde{\rho}^*(\boldsymbol{r}\tilde{\sigma}, \boldsymbol{r}'\tilde{\sigma}') & \delta(\boldsymbol{r}-\boldsymbol{r}')\delta_{\sigma\sigma'} - \rho^*(\boldsymbol{r}\tilde{\sigma}, \boldsymbol{r}'\tilde{\sigma}') \end{pmatrix}, \tag{2}$$

where the particle density matrix $\rho(\boldsymbol{r}\sigma, \boldsymbol{r}'\sigma')$ and pair density matrix $\tilde{\rho}(\boldsymbol{r}\sigma, \boldsymbol{r}'\sigma')$ are just the "11" and "12" components of $\mathcal{R}$, respectively.

The energy density functional of the Skyrme interaction is constructed with the local densities, such as the particle density $\rho(\boldsymbol{r})$, the kinetic-energy density $\tau(\boldsymbol{r})$, and the spin-orbit density $\boldsymbol{J}(\boldsymbol{r})$, etc., defined with the particle density matrix $\rho(\boldsymbol{r}\sigma, \boldsymbol{r}'\sigma')$ [31,32]. We adopt a density dependent δ interaction (DDDI) for the p-p channel:

$$v_{\text{pair}}(\boldsymbol{r}, \boldsymbol{r}') = \frac{1}{2}(1 - P_\sigma)V_0 \left[1 - \eta\left(\frac{\rho(\boldsymbol{r})}{\rho_0}\right)^\alpha\right]\delta(\boldsymbol{r}-\boldsymbol{r}'), \tag{3}$$

which presents similar properties as the pairing interaction with finite range [33]. Then the pair Hamiltonian $\tilde{h}$ is reduced to the local pair potential

$$\Delta(\boldsymbol{r}) = \frac{1}{2}V_0\left[1 - \eta\left(\frac{\rho(\boldsymbol{r})}{\rho_0}\right)^\alpha\right]\tilde{\rho}(\boldsymbol{r}), \tag{4}$$

where the local pair density $\tilde{\rho}(\boldsymbol{r})$ is defined with the pair density matrix $\tilde{\rho}(\boldsymbol{r}\sigma, \boldsymbol{r}\sigma)$ [12].

For the spherical symmetry, the generalized density matrix $\mathcal{R}$ can be expanded on the spinor spherical harmonics as

$$\mathcal{R}(\boldsymbol{r}\sigma, \boldsymbol{r}'\sigma') = \sum_{ljm} Y_{ljm}(\hat{\mathbf{r}}\sigma)\mathcal{R}_{lj}(r, r')Y^*_{ljm}(\hat{\mathbf{r}}'\sigma'). \tag{5}$$

Using the 11 and 12 components of $\mathcal{R}_{lj}$, one can write the radial local densities as

$$\rho(r) = \frac{1}{4\pi}\sum_{lj}(2j+1)\mathcal{R}^{11}_{lj}(r, r), \tag{6a}$$

$$\tau(r) = \frac{1}{4\pi}\sum_{lj}(2j+1) \times \left[\frac{\overrightarrow{d}}{dr}\mathcal{R}^{11}_{lj}(r, r')\frac{\overleftarrow{d}}{dr'} + l(l+1)\frac{\mathcal{R}^{11}_{lj}(r, r')}{rr'}\right]_{r=r'}, \tag{6b}$$

$$J(r) = \frac{1}{4\pi r}\sum_{lj}(2j+1)\left[j(j+1) - l(l+1) - \frac{3}{4}\right]\mathcal{R}^{11}_{lj}(r, r),$$

$$\tilde{\rho}(r) = \frac{1}{4\pi}\sum_{lj}(2j+1)\mathcal{R}^{12}_{lj}(r, r), \tag{6c}$$

where $\frac{\overleftarrow{d}}{dr'}$ denotes the derivative operator with respect to r' acting from right to left.

The quasiparticle wave function is represented as

$$\phi_i(\boldsymbol{r}\sigma) = \frac{1}{r}\phi_{lj}(r)Y_{ljm}(\hat{\boldsymbol{r}}\sigma), \text{ where } \phi_{lj}(r) = \begin{pmatrix}\varphi_{1,lj}(r)\\ \varphi_{2,lj}(r)\end{pmatrix}, \tag{7}$$

which obeys the radial HFB equation

$$\begin{pmatrix} -\frac{d}{dr}\frac{\hbar^2}{2m^*}\frac{d}{dr} + U_{lj}(r) - \lambda & \Delta(r) \\ \Delta(r) & \frac{d}{dr}\frac{\hbar^2}{2m^*}\frac{d}{dr} - U_{lj}(r) + \lambda \end{pmatrix}\phi_{lj}(r, E) = E\phi_{lj}(r, E). \tag{8}$$

The explicit expressions of the effective mass m^*_q and the Hartree-Fock potential $U_{lj}(r)$ can be found in Refs. [12,31], and they are constructed by the radial local densities (6) and their derivatives.

B. HFB Green's function and densities with correct asymptotic behavior

In the conventional Skyrme HFB theory, one solves the radial HFB equation (8) with the box boundary condition $\phi_{lj}(r, E) = 0$ at the edge of the box $r = R$ (R being the box size) to obtain the discretized eigensolutions for the single-quasiparticle energy and the corresponding wave functions. Then the generalized density matrix $\mathcal{R}$ can be constructed by a sum over discretized quasiparticle states. Although the box boundary condition is appropriate for the deeply bound states, it is not suitable for the weakly bound and the continuum states unless a large enough box size is taken.

Here the Green's function method is used to impose the correct asymptotic behaviors on the wave functions especially for the continuum states, and to calculate the densities.

The HFB Green's function $\mathcal{G}_{0,lj}(r, r', E)$ can be constructed with solutions of the radial HFB equation (8). Suppose $\phi^{(rs)}_{lj}(r, E)$ and $\phi^{(+s)}_{lj}(r, E)$ ($s = 1, 2$) are independent solutions of the HFB equation (8) that satisfy the boundary conditions at the origin and at the edge of the box, $r = R$, respectively, then the HFB Green's function is given by [13,34]

$$\mathcal{G}_{0,lj}(r, r', E) = \sum_{s,s'=1,2} c^{ss'}_{lj}(E)\big[\theta(r-r')\phi^{(+s)}_{lj}(r, E)\phi^{(rs')T}_{lj}(r', E) + \theta(r'-r)\phi^{(rs')}_{lj}(r, E)\phi^{(+s)T}_{lj}(r', E)\big]. \tag{9}$$

The coefficients $c^{ss'}_{lj}(E)$ are expressed in terms of the Wronskians as

$$\begin{pmatrix} c^{11}_{lj} & c^{12}_{lj} \\ c^{21}_{lj} & c^{22}_{lj}\end{pmatrix} = \begin{pmatrix} w_{lj}(r1, +1) & w_{lj}(r1, +2) \\ w_{lj}(r2, +1) & w_{lj}(r2, +2)\end{pmatrix}^{-1} \tag{10}$$

with

$$w_{lj}(rs, +s') = \frac{\hbar^2}{2m}\left[\varphi^{(rs)}_{1,lj}(r)\frac{d}{dr}\varphi^{(+s')}_{1,lj}(r) - \varphi^{(+s')}_{1,lj}(r)\frac{d}{dr}\varphi^{(rs)}_{1,lj}(r) - \varphi^{(rs)}_{2,lj}(r)\frac{d}{dr}\varphi^{(+s')}_{2,lj}(r) + \varphi^{(+s')}_{2,lj}(r)\frac{d}{dr}\varphi^{(rs)}_{2,lj}(r)\right]. \tag{11}$$

To impose the correct asymptotic behavior on the wave function for the continuum states, we adopt the boundary condition as follows:

$$\begin{cases}\phi^{(rs)}_{lj}(r, E): & \text{regular at the origin } r = 0\\ \phi^{(+s)}_{lj}(r, E): & \text{outgoing wave at } r \to \infty\end{cases}, \tag{12}$$

Explicitly, the solutions $\phi_{lj}^{(+s)}(r,E)$ at $r > R$ satisfy

$$\phi_{lj}^{(+1)}(r,E) \to \begin{pmatrix} e^{ik_+(E)r} \\ 0 \end{pmatrix}, \quad \phi_{lj}^{(+2)}(r,E) \to \begin{pmatrix} 0 \\ e^{ik_-(E)r} \end{pmatrix}. \quad (13)$$

Here $k_\pm(E) = \sqrt{2m(\lambda \pm E)}/\hbar$ and their branch cuts are chosen so that $\mathrm{Im}k_\pm > 0$ is satisfied.

The generalized density matrix can be obtained by the contour integral of the Green's function on the complex quasiparticle energy plane, which in the spherical case can be written as [13,34]

$$\mathcal{R}_{lj}(r,r') = \frac{1}{2\pi i}\oint_{C_E} dE \frac{\mathcal{G}_{0,lj}(r,r',E)}{rr'}. \quad (14)$$

The contour C_E should be chosen to enclose the negative energy part of the quasiparticle spectra, as shown in Fig. 1, so that all the quasiparticle states inside the contour are summed up. Here the discrete quasiparticle states are denoted by crosses above the Fermi energy λ. Below the Fermi energy, the continuum quasiparticle states are denoted by the solid stripe. As a result, the radial local densities (6) can be calculated by the contour integral of the radial Green's function. In this way, we realize a fully self-consistent continuum Skyrme HFB calculations.

C. Numerical details

For the Skyrme interaction, we choose the parameter set SLy4 [35], and for the pairing interaction the DDDI parameters in Eq. (4) are adopted as $V_0 = -458.4$ MeV fm^{-3}, $\eta = 0.71$, $\alpha = 0.59$, and $\rho_0 = 0.08$ fm^{-3} [36–38]. They reproduce the experimental neutron pairing gap along the Sn isotopic chain. We remark also that the parameter V_0 is chosen in such a way that the DDDI reproduces the ^1S scattering length $a = -18.5$ fm of the bare nuclear force in the low density limit $\rho(r) \to 0$, i.e., in the free space outside the nucleus. Because of this constraint and the density dependence, the pairing interaction strength is large around the surface, and even increases in the exterior. The truncation of the quasiparticle states is up to the angular momentum $l = 12$ and $j = 25/2$ and to the maximal quasiparticle energy $E_{\mathrm{cut}} = 60$ MeV.

For the contour integration of the Green's function, the path C_E is chosen to be a rectangle as shown in Fig. 1 with the height $\gamma = 1$ MeV and the length $E_{\mathrm{cut}} = 60$ MeV, which symmetrically encloses the real negative quasiparticle energy axis. For the contour integration we adopt an energy step $\Delta E = 0.01$ MeV on the contour path. We have checked that for the choice of these contour path parameters, the precision for $\rho(r)$ and $\tilde{\rho}(r)$ thus obtained are up to 10^{-10} fm^{-3} and 10^{-9} fm^{-3}, respectively. We choose the box size $R = 20$ fm, and the mesh size $\Delta r = 0.2$ fm. We have also checked that dependence of the results on the box size is very small thanks to the boundary condition (13) with proper asymptotic form.

III. RESULTS AND DISCUSSION

In this section, taking the isotonic chain $N = 86$ as an example, we will discuss in detail how characters of the weakly bound and unbound quasiparticle states of neutrons vary as the neutron Fermi energy approaches zero, and how they contribute to the pair correlation.

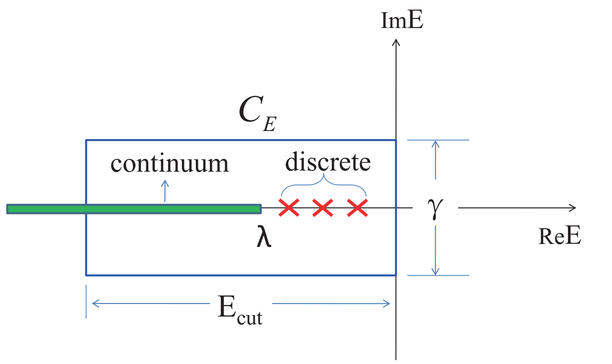

FIG. 1. (Color online) Contour path C_E to perform the integration of the Green's function on the complex quasiparticle energy plane. The path is chosen to be a rectangle with the height γ and the length E_{cut}. The crosses denote the discrete quasiparticle states. The continuum states are denoted by the solid stripe below the Fermi energy λ.

A. HFB ground states and the quasiparticle spectra

Some properties of the HFB ground state for ^{136}Sn, ^{134}Cd, ^{132}Pd, ^{130}Ru, and ^{128}Mo are listed in the first four rows in Table I. The neutron Fermi energy (the first row) monotonically increases from -2.39 MeV in ^{136}Sn to -0.42 MeV in ^{128}Mo as the proton number Z decreases. This is because the neutron Hartree-Fock potential becomes more shallow as Z decreases, and we could not find a self-bound HFB solution (with $\lambda < 0$) in ^{126}Zr and lighter isotones.

Table I also shows the total neutron pair correlation energy

$$E_{\mathrm{pair}} = \frac{1}{2}\int d\boldsymbol{r}\Delta(\boldsymbol{r})\tilde{\rho}(\boldsymbol{r}), \quad (15)$$

and the average pairing gap

$$\Delta_{uv} = \frac{\int d\boldsymbol{r}\Delta(\boldsymbol{r})\tilde{\rho}(\boldsymbol{r})}{\int d\boldsymbol{r}\tilde{\rho}(\boldsymbol{r})}. \quad (16)$$

The quantity in the denominator is the total neutron "pair number"

$$\tilde{N} = \int \tilde{\rho}(\boldsymbol{r})d\boldsymbol{r}, \quad (17)$$

which represents the amount of the pair condensate. In the following, we will present the discussion about the absolute value of pair density $\tilde{\rho}$ and the corresponding $\tilde{N}$. It is noted that the variation of the average pairing gap and the total pair correlation energy along the isotones is less than 10% from ^{136}Sn to the last bound nucleus ^{128}Mo.

It is useful to investigate properties of individual quasiparticle states which are the elementary mode of single-particle motion in the HFB theory and the building blocks of the pair density. It is noted that the spectrum of the quasiparticles, i.e., the eigenstates of the HFB equation, includes both the discrete $(0 < E < |\lambda|)$ and continuum $(E > |\lambda|)$ quasiparticle states.

TABLE I. Neutron threshold energy $|\lambda|$, total average pairing gap $\Delta_{uv}^{\rm tot}$, pair number $\tilde{N}^{\rm tot}$, and pair correlation energy $E_{\rm pair}^{\rm tot}$ in the $N = 86$ isotones are listed in the first four rows. The following rows list properties of the individual low-lying quasiparticle states shown in Fig. 2: the peak energy $E_{\rm qp}$ and the width Γ extracted from the pair number density $\tilde{n}_{lj}(E)$, the Hartree-Fock single-particle energy ε corresponding to the quasiparticle state, the pair number $\tilde{N}'_{nlj}$, the pair correlation energy $E'_{{\rm pair},nlj}$, and the effective pairing gap $\Delta'_{uv,nlj}$ evaluated for the quasiparticle state lj within the energy interval $E = 0 \sim 4$ MeV. The unit of the energy is MeV, except for the width Γ shown in keV.

		^{136}Sn	^{134}Cd	^{132}Pd	^{130}Ru	^{128}Mo
	$\|\lambda\|$	2.390	1.884	1.383	0.894	0.421
	$\Delta_{uv}^{\rm tot}$	0.736	0.721	0.707	0.694	0.678
	$\tilde{N}^{\rm tot}$	16.875	17.083	17.458	18.111	19.245
	$E_{\rm pair}^{\rm tot}$	−6.212	−6.162	−6.173	−6.280	−6.527
$2f_{7/2}$	ε	−2.302	−1.799	−1.297	−0.801	−0.309
	$E_{\rm qp}$	0.760	0.749	0.740	0.734	0.733
	Γ	< 0.1	0.1	< 0.1	2.5	7.3
	$\Delta'_{uv,nlj}$	0.755	0.745	0.737	0.731	0.727
	$\tilde{N}'_{nlj}$	3.951	3.954	3.959	3.966	3.973
	$E'_{{\rm pair},nlj}$	−1.492	−1.473	−1.458	−1.449	−1.445
$3p_{3/2}$	ε	−0.480	−0.235	−0.010	0.190	0.362
	$E_{\rm qp}$	1.965	1.685	1.365	1.081	0.803
	Γ	< 0.1	< 0.1	95.0	238.8	396.4
	$\Delta'_{uv,nlj}$	0.591	0.579	0.568	0.554	0.529
	$\tilde{N}'_{nlj}$	0.528	0.591	0.679	0.813	1.040
	$E'_{{\rm pair},nlj}$	−0.156	−0.171	−0.193	−0.225	−0.275
$3p_{1/2}$	ε	0.066	0.257	0.423	0.563	0.678
	$E_{\rm qp}$	2.405	2.089	1.760	1.422	1.071
	Γ	122.3	264.7	427.4	612.2	802.0
	$\Delta'_{uv,nlj}$	0.570	0.553	0.540	0.522	0.501
	$\tilde{N}'_{nlj}$	0.179	0.199	0.226	0.268	0.339
	$E'_{{\rm pair},nlj}$	−0.051	−0.055	−0.061	−0.070	−0.085
$2f_{5/2}$	ε	0.449	0.862	1.237	1.559	1.816
	$E_{\rm qp}$	2.919	2.820	2.694	2.540	2.364
	Γ	21.7	50.6	110.1	223.8	431.9
	$\Delta'_{uv,nlj}$	0.736	0.721	0.708	0.696	0.685
	$\tilde{N}'_{nlj}$	0.690	0.682	0.684	0.701	0.736
	$E'_{{\rm pair},nlj}$	−0.254	−0.246	−0.242	−0.244	−0.252
$1h_{9/2}$	ε	0.566	1.215	1.869	2.522	3.163
	$E_{\rm qp}$	3.051	3.186	3.334	3.492	3.661
	Γ	0.3	0.8	2.2	7.0	24.2
	$\Delta'_{uv,nlj}$	0.766	0.756	0.751	0.748	0.747
	$\tilde{N}'_{nlj}$	1.214	1.145	1.079	1.016	0.948
	$E'_{{\rm pair},nlj}$	−0.465	−0.433	−0.405	−0.380	−0.354

Accordingly, the pair density can be expressed as a sum of contributions from individual quasiparticle states as

$$\tilde{\rho}(r) = \sum_{nlj,E_{nlj}<|\lambda|} \tilde{\rho}_{nlj}(r) + \sum_{lj} \int_{|\lambda|}^{E_{\rm cut}} \tilde{\rho}_{lj}(r, E)dE, \quad (18)$$

where the first term in the right-hand side is the sum over the discrete states, and the second term represents the integral of the contribution to the pair density $\tilde{\rho}(r)$ from the continuum quasiparticle state with quantum number lj at energy E. If we include the discrete quasiparticle states in the definition of $\tilde{\rho}_{lj}(r, E)$, the above equation can be expressed as

$$\tilde{\rho}(r) = \sum_{lj} \tilde{\rho}_{lj}(r), \quad \text{where } \tilde{\rho}_{lj}(r) = \int_0^{E_{\rm cut}} \tilde{\rho}_{lj}(r, E)dE, \quad (19)$$

and $\tilde{\rho}_{lj}(r, E)$ can be calculated as

$$\tilde{\rho}_{lj}(r, E) = \left(\frac{2j+1}{4\pi r^2}\right) \frac{1}{\pi} {\rm Im}\mathcal{G}_{0,lj}^{(12)}(r, r, -E - i\epsilon). \quad (20)$$

We can also calculate contributions from the state with quantum number lj at energy E to the pair number $\tilde{N}$ as

$$\tilde{n}_{lj}(E) = \int 4\pi r^2 \tilde{\rho}_{lj}(r, E)dr, \quad (21)$$

which satisfies

$$\tilde{N} = \sum_{lj} \int_0^{E_{\rm cut}} \tilde{n}_{lj}(E)dE. \quad (22)$$

We call the quantity $\tilde{n}_{lj}(E)$ the "pair number density" in the following. We can also calculate the "occupation number density" $n_{lj}(E) = \int 4\pi r^2 \rho_{lj}(r, E)dr$, which is discussed in Refs. [16,21–25]. In the following, we will investigate the pair number density $\tilde{n}_{lj}(E)$ rather than the occupation number density $n_{lj}(E)$ since we found that the pair number density $\tilde{n}_{lj}(E)$ represents more clearly the structure of continuum quasiparticle states relevant to the pair correlation.

With the smoothing parameter ϵ in Eq. (20) the δ function (no width) originating from a discrete quasiparticle state is simulated by a Lorentzian function with the full-width at half-maximum (FWHM) of 2ϵ. In the following calculation, we take $\epsilon = 5$ keV to discuss the structure of pair number density. Subtracting the smoothing width $2\epsilon = 10$ keV from the FWHM of the peak, we obtain the physical width Γ of the peak.

Figure 2 shows the pair number densities $\tilde{n}_{lj}(E)$ for neutron quasiparticle states in a low-lying energy interval $E = 0 \sim 4$ MeV in the $N = 86$ isotones. A peak structure below the threshold energy $E = |\lambda|$ (the dashed vertical line) is a discrete quasiparticle state (simulated by the Lorentzian function), and a peak above the dashed line may be identified as a quasiparticle resonance. The width Γ of the peak as well as the peak energy $E_{\rm qp}$ are tabulated in Table I. In the same table, we also show the corresponding Hartree-Fock single-particle energy ε, which is the eigensolution of the Hartree-Fock single-particle Hamiltonian h obtained with the box boundary condition. An eigenstate with $\varepsilon < 0$ is discrete (bound) single-particle orbit, and $\varepsilon > 0$ is discretized continuum single-particle orbit whose energy gives an estimate for the Hartree-Fock single-particle resonance energy.

In ^{136}Sn, the quasiparticle states corresponding to weakly bound Hartree-Fock single-particle states, $2f_{7/2}$ and $3p_{3/2}$, are discrete states with no width (less than 0.1 keV in the actual numerical calculation) as they are located below the threshold energy $|\lambda|$. The Hartree-Fock single-particle state $3p_{1/2}$ is already in the continuum ($\varepsilon \sim 70$ keV), and forms a

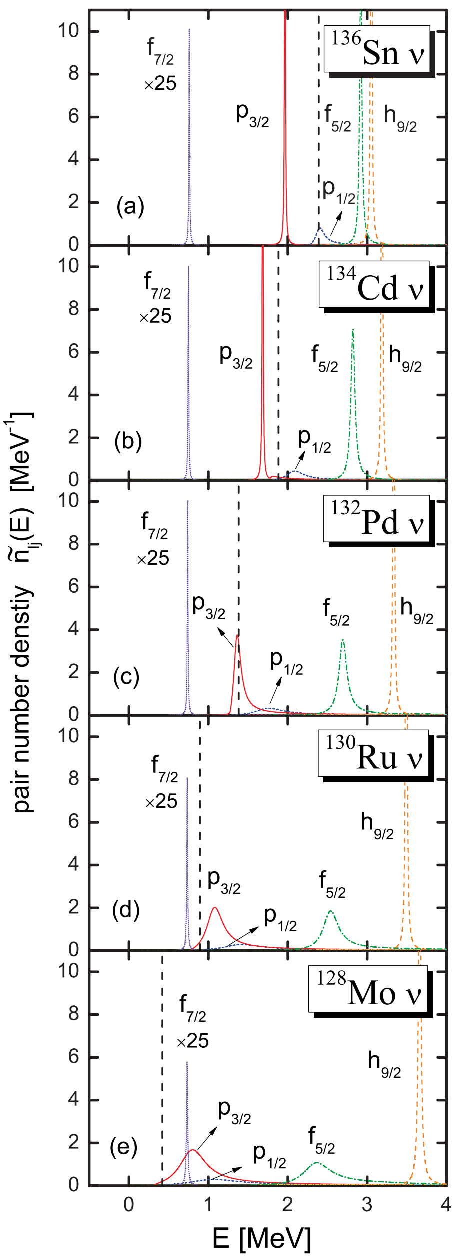

FIG. 2. (Color online) Pair number densities $\tilde{n}_{lj}(E)$ of neutron quasiparticle states with different lj around the threshold energy in the $N = 86$ isotones, obtained with the self-consistent continuum Skyrme HFB theory using Green's function method. The thick dashed line denotes the threshold energy $|\lambda|$ for the continuum quasiparticle states. The density of state for $f_{7/2}$ is divided by a factor of 25.

quasiparticle resonance located just above the threshold energy with $E_{\mathrm{qp}} \sim |\lambda| + 15$ keV with a large width $\Gamma = 122$ keV. On the contrary, the peaks for higher angular momentum states, e.g., $2f_{5/2}$ and $1h_{9/2}$, have finite but smaller widths, forming narrow quasiparticle resonances.

As the proton number decreases, the neutron potential becomes shallower, and both the Fermi energy and the single-particle energies are raised up. The width grows larger in ^{134}Cd than in ^{136}Sn for all the quasiparticle resonances above the threshold, although the weakly bound single-particle states $2f_{7/2}$ and $3p_{3/2}$ remain the discrete states in the quasiparticle spectrum.

When the Fermi energy is raised up further in ^{132}Pd, the $3p_{3/2}$ quasiparticle state becomes a resonance located just around the threshold energy, with a large width 95 keV. Since the corresponding Hartree-Fock state is still bound (although the binding energy is very small, $\varepsilon \sim -10$ keV), it is the pair correlation that makes the corresponding quasiparticle state unbound with the finite width.

In ^{130}Ru, the single-particle energies are raised further. All the single-particle orbits under discussion except $2f_{7/2}$ become unbound. Correspondingly the widths of the quasiparticle resonances $3p_{3/2}$, $3p_{1/2}$, $2f_{5/2}$, and $1h_{9/2}$ grow also.

When we come to the last bound nucleus ^{128}Mo in this isotonic chain, all the quasiparticle states lie in the continuum. It is noticed that both the $3p_{3/2}$ and $3p_{1/2}$ quasiparticle states become very broad resonances whose width is comparable with the resonance energy $E_{\mathrm{qp}} - |\lambda|$ measured from the threshold. The quasiparticle state $2f_{7/2}$ is now a quasiparticle resonance embedded in the continuum although the Hartree-Fock single-particle state $2f_{7/2}$ is still a bound orbit. The width comes from the continuum coupling caused by the pair correlation, as the $3p_{3/2}$ state in ^{132}Pd. The continuum coupling effect is much larger for the $3p_{3/2}$ state than $2f_{7/2}$, as is seen in the considerably different values of the width.

B. Pairing effects on the resonance width

The large widths of the $3p_{1/2}$ and $3p_{3/2}$ quasiparticle resonances have two origins. One is the barrier penetration of the Hartree-Fock plus centrifugal potential, which is low for the states with low angular momentum (the barrier height of the $p_{1/2}$ and $p_{3/2}$ states in ^{128}Mo is 0.351 and 0.344 MeV, respectively). This is effective even without the pair correlation. The other is the presence of the pair potential, because of which even a bound single-particle orbit can couple with continuum states, then forms a quasiparticle resonance. The latter effect may be seen by examining the pair number density $\tilde{n}_{lj}(E)$ under a variation of the strength of the effective pairing interaction.

Table II shows the quasiparticle resonance widths in ^{128}Mo obtained with different pairing interaction parameter $\eta = 0.84$, 0.71, and 0.62 in Eq. (3). It is seen that for the changes of the average pairing gap $\Delta_{uv} = 0.41 \sim 0.68 \sim 1.08$ MeV, the variation of the widths of the $3p_{1/2}$ and $3p_{3/2}$ quasiparticle resonances are $\Gamma = 0.73 \sim 0.80 \sim 0.94$ MeV and $0.34 \sim 0.40 \sim 0.49$ MeV, respectively. We deduce that the pairing effect on the widths are approximately ~ 100 keV for $3p_{1/2}$, and a slightly smaller for $3p_{3/2}$. A comparably large pairing effect is also seen in the width of $2f_{5/2}$ quasiparticle resonance where the corresponding Hartree-Fock single-particle state is a broad resonance already without the pair correlation. (On the contrary, the pairing effect is not large for the other quasiparticle resonances arising from the hole orbits and those with narrow resonances.) The pair correlation increases significantly the width of the quasiparticle resonances corresponding to weakly bound orbits with low angular momentum or to the Hartree-Fock single-particle resonances close to the barrier top. Since the wave functions of these quasiparticle resonances

TABLE II. Dependence of the ground-state pair correlation and the quasiparticle properties in ^{128}Mo on the pairing interaction strength. To control the pairing interaction strength, we vary the parameter η of DDDI in Eq. (3) as $\eta = 0.84, 0.71, 0.62, 0.56$. We list here the threshold energy $|\lambda|$, the total average pairing gap Δ_{uv}, and the total pair correlation energy $E_{\rm pair}$, the peak energy $E_{\rm qp}$, and the width Γ of the lowest two quasiparticle resonances for $p_{3/2}$, $p_{1/2}$, $f_{5/2}$, and $f_{7/2}$. The unit of energy is MeV, except for the width Γ shown in keV.

η		0.84	0.71	0.62	0.56
	$\|\lambda\|$	0.363	0.421	0.572	0.778
	$\Delta_{uv}^{\rm tot}$	0.414	0.678	1.077	1.541
	$E_{\rm pair}^{\rm tot}$	−2.860	−6.527	−13.902	−24.800
$2f_{7/2}$	ε	−0.330	−0.309	−0.292	−0.283
	$E_{\rm qp}$	0.428	0.733	1.146	1.591
	Γ	4.0	7.3	13.9	24.6
$1f_{7/2}$	ε	−25.566	−25.571	−25.562	−25.534
	$E_{\rm qp}$	25.204	25.155	25.013	24.812
	Γ	0.4	0.4	0.1	1.6
$3p_{3/2}$	ε	0.355	0.362	0.369	0.373
	$E_{\rm qp}$	0.670	0.803	1.049	1.346
	Γ	337.7	396.4	492.4	612.6
$2p_{3/2}$	ε	−20.175	−20.151	−20.114	−20.078
	$E_{\rm qp}$	19.816	19.742	19.579	19.379
	Γ	0.9	3.1	9.1	19.9
$3p_{1/2}$	ε	0.673	0.678	0.682	0.685
	$E_{\rm qp}$	0.962	1.070	1.290	1.569
	Γ	727.4	802.0	936.2	1127.7
$2p_{1/2}$	ε	−18.553	−18.528	−18.494	−18.463
	$E_{\rm qp}$	18.194	18.119	17.960	17.768
	Γ	2.2	5.6	13.5	25.4
$2f_{5/2}$	ε	1.817	1.816	1.814	1.811
	$E_{\rm qp}$	2.260	2.365	2.594	2.899
	Γ	392.9	431.9	514.4	660.0
$1f_{5/2}$	ε	−20.970	−21.007	−21.040	−21.048
	$E_{\rm qp}$	20.609	20.595	20.498	20.338
	Γ	0.2	0.5	2.5	7.4

have significant amplitude in the barrier region, the influence of the pair potential on the continuum coupling can be effective.

C. Contribution of continuum quasiparticle states to the pair correlation

Let us now investigate how the quasiparticle resonances, shown in Fig. 2, contribute to the neutron pair correlation.

For this purpose, we examine their contribution to the neutron pair density in the low-lying energy interval $E = 0 \sim 4$ MeV. We denote $\tilde{\rho}'_{nlj}(r)$ for the partial contribution from the low-lying quasiparticle state, and evaluate it by performing the integral in Eq. (19) with $E_{\rm cut} = 4$ MeV for the quasiparticle resonances $2f_{7/2}, 3p_{3/2}, 3p_{1/2}$, etc. The quantity weighted with the volume element, $4\pi r^2\tilde{\rho}'_{nlj}(r)$, is shown in Fig. 3 for the $N = 86$ isotones.

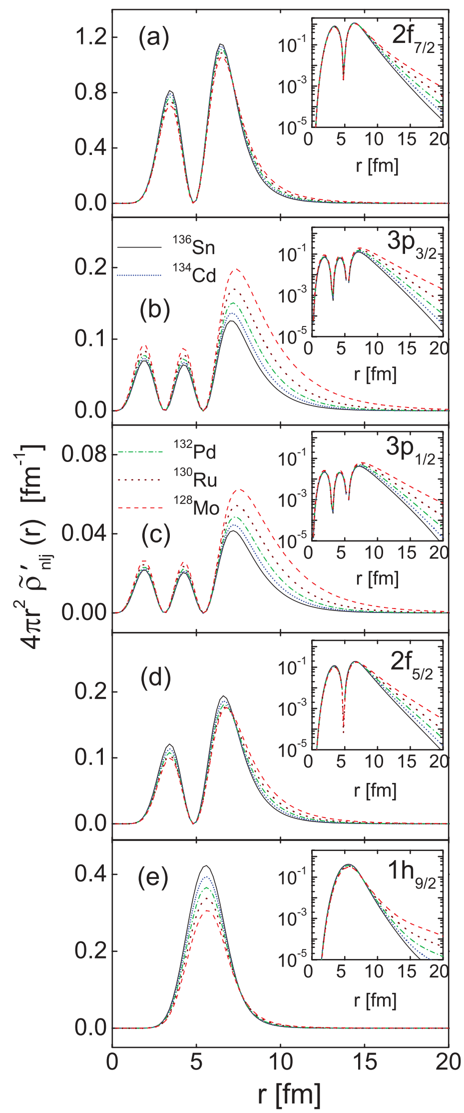

FIG. 3. (Color online) Neutron pair density $4\pi r^2\tilde{\rho}'_{nlj}(r)$ contributed by the low-lying quasiparticle states shown in Fig. 2 for the $N = 86$ isotones,where $\tilde{\rho}'_{nlj}(r) = \int_0^{4\,\rm MeV} dE\,\tilde{\rho}_{lj}(r,E)$.The inserts present the same density distribution in a log scale.

As the nucleus becomes more and more weakly bound from ^{136}Sn to ^{128}Mo, a significant variation of the pair density $\tilde{\rho}'_{nlj}(r)$ is seen for the $3p_{3/2}$ and $3p_{1/2}$ states: the amplitude of $\tilde{\rho}'_{nlj}(r)$ increases dramatically at the positions far outside the surface, $r \approx 7$–15 fm. For the $3p_{1/2}$ state, the increases at $r = 8$ and 10 fm are 80% and 200%, respectively, while the increase inside, e.g., at $r = 2$ fm, is only $\sim 20\%$. The other quasiparticle states $2f_{7/2}, 2f_{5/2}$, and $1h_{9/2}$ exhibit a similar trend of extending outside but to a much weaker extent.

Evaluating the volume integral of $\tilde{\rho}'_{nlj}(r)$, we list in Table I the quantity $\tilde{N}'_{nlj} = \int 4\pi r^2\tilde{\rho}'_{nlj}(r)dr$, which represents a contribution to the pair number $\tilde{N}$ from the low-lying quasiparticle states. It is clear that the pair number $\tilde{N}'_{nlj}$ of the $3p_{3/2}$ and $3p_{1/2}$ states in the most weakly bound ^{128}Mo is twice as big as those in ^{136}Sn, as a result of the obvious increase of $\tilde{\rho}'_{nlj}(r)$ at the positions $r \approx 7$–15 fm.

We show also in Table I a partial contribution

$$E'_{\mathrm{pair},nlj} = \frac{1}{2}\int 4\pi r^2 dr\,\Delta(r)\tilde{\rho}'_{nlj}(r) \quad (23)$$

to the pair correlation energy from the low-lying quasiparticle state. It can be seen that, moving from ^{136}Sn to ^{128}Mo, the contributions of the $3p_{1/2}$ and $3p_{3/2}$ states do increase up to around 70%. It is clear that this increase of the pair correlation energy is due to not only the increase in $\tilde{\rho}'_{nlj}(r)$ but also the large spatial overlap between the pair density $\tilde{\rho}'_{nlj}(r)$ and the pair potential $\Delta(r)$. In Fig. 4 we show the neutron pair potential $\Delta(r)$ and the product of the pair potential and the pair density $4\pi r^2\Delta(r)\tilde{\rho}'_{nlj}(r)$, the integrand of the pair correlation energy, Eq. (23). Since the radial profile of the pair potential $\Delta(r)$ is not only surface-peaked but also extends up to $r \sim 10$ fm, the two quantities have significant overlap, and hence the product $4\pi r^2\Delta(r)\tilde{\rho}'_{nlj}(r)$ exhibits a significant increase at $r \approx 7 - 10$ fm. This brings about a large increase of the pair correlation energy.

We note here that the energies of the Hartree-Fock single-particle orbits corresponding to the $3p_{3/2}$ and $3p_{1/2}$ states move upward around and beyond the threshold: from $\varepsilon = -0.48$ MeV (weakly bound) to ≈ 0.36 MeV (unbound with the single-particle energy comparable with the barrier height ≈ 0.34 MeV) in the $3p_{3/2}$ case, and from ≈ 0.07 MeV (around the threshold) to ≈ 0.68 MeV (even above the barrier height ≈ 0.35 MeV) in the $3p_{1/2}$ case. In the least bound case (^{128}Mo), the $3p_{3/2}$ and $3p_{1/2}$ quasiparticle resonances have the widths $\Gamma = 0.396$ and 0.802 MeV, respectively, which are comparable with the resonance energy. Nevertheless, both the pair number $\tilde{N}'_{nlj}$ and the pair correlation energy $E'_{\mathrm{pair},lj}$ continue to increase as is seen above. This indicates that the weakly bound and unbound states can feel the pair potential and contribute to the pair correlation in sizable way.

D. Effective pairing gap of continuum quasiparticle states

In order to make a quantitative estimate for the influence of the pair potential on the low-lying quasiparticle states, we evaluate the state-dependent effective pairing gap which can be defined by

$$\Delta'_{uv,nlj} = \frac{\int 4\pi r^2\Delta(r)\tilde{\rho}'_{nlj}(r)dr}{\int 4\pi r^2\tilde{\rho}'_{nlj}(r)dr} = -2E'_{\mathrm{pair},nlj}/\tilde{N}'_{nlj} \quad (24)$$

using the pair density $\tilde{\rho}'_{nlj}(r)$ for the specific quasiparticle state. We list it in Table I.

In the nucleus ^{136}Sn, the effective pairing gaps of the $3p_{3/2}$ and $3p_{1/2}$ states are $\Delta'_{uv,nlj} = 0.591$ MeV and 0.570 MeV, respectively, which are about $77 \sim 80$ % of the total-average pairing gap $\Delta^{\mathrm{tot}}_{uv} = 0.736$ MeV. The effective pairing gaps still keep finite values of the same order in the last bound nucleus ^{128}Mo, where the $3p_{1/2}$ and $3p_{3/2}$ Hartree-Fock orbits are both unbound. For the $3p_{3/2}$ state, the effective pairing gap is $\Delta'_{uv,nlj} = 0.529$ MeV. It stays at the level of 78% of the average gap $\Delta^{\mathrm{tot}}_{uv} = 0.678$ MeV. Even for the $3p_{1/2}$ resonance with large width, the effective pairing gap 0.501 MeV keeps 74% of the total. The variation of the effective pairing gaps of the $3p$ states from ^{136}Sn to ^{128}Mo is also small, i.e., they decrease only slightly by $\sim 10\%$.

The facts that the effective pairing gaps of the $3p_{3/2}$ and $3p_{1/2}$ states are slightly smaller than the total average value, and that they decrease as the orbits become less bound and become unbound in the continuum, can be ascribed to the decoupling effect [21–24], which is expected to originate from the possible small overlap between the single-particle wave function and the pair potential. In Ref. [23], the effective pairing gap in the weakly bound p orbit is suggested to be less than 50% of the average, and possibly less than 1/3 for an unbound p orbit. Compared with these numbers, the decoupling effect observed here ($\approx$ 20–25 %) is much smaller. Namely, we can see that these quasiparticle states persist to feel the pair potential and contribute to the pair correlation even if they become unbound and have large width.

The difference between the conclusions of our analysis and those of Ref. [23] can be explained as follows. In our analysis, the self-consistent pair potential not only peaks around the surface ($r \approx 5$–7 fm), but also extends outside (up to 10 fm or more) as shown in Fig. 4(a), whereas the pair potential in Refs. [21–24] has a Woods-Saxon shape whose main part is concentrated inside the nucleus. Meanwhile, the pair density $4\pi r^2\tilde{\rho}'_{nlj}(r)$ also peaks around the surface and extends outside. Let us take, for instance, the $3p_{1/2}$ resonance state in ^{128}Mo whose Hartree-Fock single-particle energy is around 0.7 MeV. Considering the wave function of the quasiparticle state at the peak energy E_{qp}, its upper component $\varphi_1(r, E_{\mathrm{qp}})$ has large amplitude around the barrier as the state is located above the barrier height (0.35 MeV), and it oscillates in the asymptotic region. On the other hand, the lower component $\varphi_2(r, E_{\mathrm{qp}})$ exhibits an exponentially decaying asymptotics $\propto \exp(-\kappa r)$ with $\kappa = \sqrt{2m(|\lambda| + E_{\mathrm{qp}})}/\hbar$ [15]. Since the contribution of

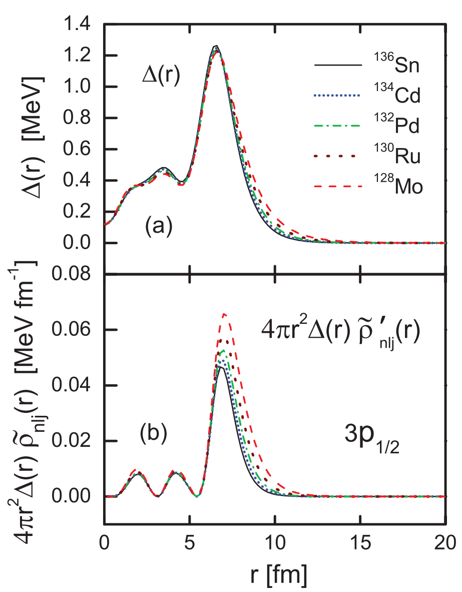

FIG. 4. (Color online) (a) Neutron pair potential $\Delta(r)$ in the $N = 86$ isotones, and (b) integrand of the corresponding pair correlation energy, $4\pi r^2\Delta(r)\tilde{\rho}'_{nlj}(r)$, for the $3p_{1/2}$ quasiparticle state, where the pair density $\tilde{\rho}'_{nlj}(r)$ is the contribution from the $3p_{1/2}$ resonant quasiparticle state which is shown in Fig. 3.

this state to the pair density $\tilde{\rho}'_{nlj}(r)$ is given by the product of $\varphi_1(r, E_{\rm qp})$ and $\varphi_2(r, E_{\rm qp})$, the pair density is confined around the nucleus ($r \lesssim 15$ fm in the present numerical examples) and the largest amplitude of $4\pi r^2 \tilde{\rho}'_{nlj}(r)$ shows up around the surface even though the quasiparticle state is located far above the threshold and has a large width. Consequently, such states have sizable overlap with the pair potential and thus keep the finite effective pairing gap even when the nucleus becomes more weakly bound.

Conversely we may argue a condition for the occurrence of the strong decoupling in a semiquantitative way. Since the spatial extension of the pair density is characterized by a size constant $r_{\tilde{\rho}} \equiv 1/\kappa = \hbar/\sqrt{2m(|\lambda| + E_{\rm qp})}$, the strong decoupling can be expected when $r_{\tilde{\rho}} \gg R_{\rm surf.}$, i.e., only when both the Fermi energy $|\lambda|$ and the quasiparticle energy $E_{\rm qp}$ are sufficiently small. Here the energy $E_{\rm qp}$ of a discrete or resonance quasiparticle state has a lower bound $E_{\rm qp} \gtrsim \Delta'_{nlj}$ given by the effective pairing gap. For the p states in ^{128}Mo, we find $E_{\rm qp} \sim 0.7$ MeV, and $|\lambda| > 0.4$ MeV, therefore, $r_{\tilde{\rho}} \sim 4$ fm, which is not much larger than the nuclear radius $R_{\rm surf} \sim 5$ fm. This explains why the decoupling is weak here.

E. The volume pairing

The relation between the present results and the decoupling scenario in Refs. [21–24] may be clarified by examining a case where the pairing potential has a radial dependence similar to that adopted in those references. We have repeated the same continuum HFB calculation except that we now employ the so-called volume pairing, in which the DDDI parameters in Eq. (4) are chosen so that the effective pairing force has no density dependence ($\eta = 0$), and the strength $V_0 = -205.0$ MeV fm^{-3} reproduces the overall value of the total average pairing gap $\Delta^{\rm tot}_{uv}$ listed in Table I. The results are shown in Fig. 5 and Table III.

TABLE III. The same as Table I, but for the volume pairing. Here only the ground-state properties and the properties of the $3p_{3/2}$ and $3p_{1/2}$ quasiparticle states are listed.

		^{136}Sn	^{134}Cd	^{132}Pd	^{130}Ru	^{128}Mo
	$\|\lambda\|$	2.355	1.833	1.323	0.829	0.356
	$\Delta^{\rm tot}_{uv}$	0.771	0.738	0.705	0.672	0.635
	$\tilde{N}^{\rm tot}$	15.266	14.992	14.788	14.688	14.777
	$E^{\rm tot}_{\rm pair}$	−5.884	−5.534	−5.216	−4.932	−4.694
	ε	−0.471	−0.216	0.009	0.204	0.367
	$E_{\rm qp}$	1.924	1.630	1.292	0.986	0.676
	Γ	0.1	0.1	86.9	222.9	357.9
$3p_{3/2}$	$\Delta'_{uv,nlj}$	0.558	0.523	0.486	0.442	0.392
	$\tilde{N}'_{nlj}$	0.452	0.486	0.535	0.615	0.766
	$E'_{{\rm pair},nlj}$	−0.126	−0.127	−0.130	−0.136	−0.150
	ε	0.073	0.271	0.437	0.573	0.682
	$E_{\rm qp}$	2.363	2.034	1.693	1.341	0.973
	Γ	118.9	265.5	428.1	607.3	789.1
$3p_{1/2}$	$\Delta'_{uv,nlj}$	0.528	0.487	0.451	0.415	0.370
	$\tilde{N}'_{nlj}$	0.144	0.152	0.164	0.183	0.216
	$E'_{{\rm pair},nlj}$	−0.038	−0.037	−0.037	−0.038	−0.040

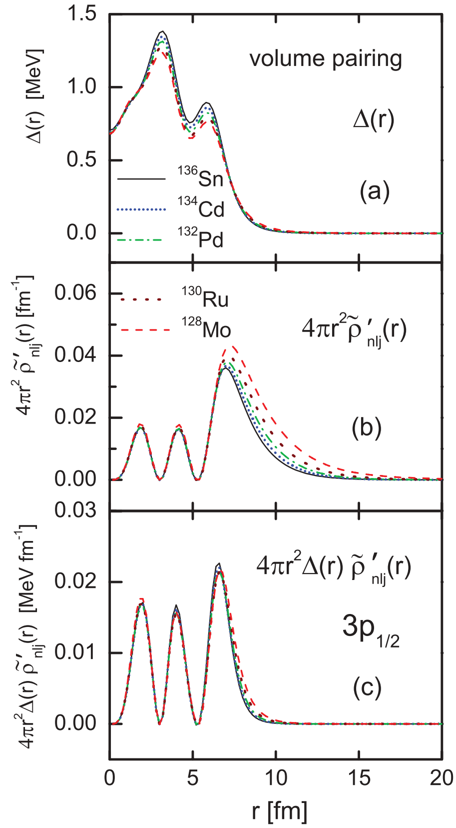

FIG. 5. (Color online) (a) Neutron pair potential $\Delta(r)$, (b) neutron pair density $4\pi r^2 \tilde{\rho}'_{nlj}(r)$ for the $3p_{1/2}$ quasiparticle state, where $\tilde{\rho}'_{nlj}(r) = \int_0^{4\,\rm MeV} dE\, \tilde{\rho}_{lj}(r, E)$, and (c) integrand of the corresponding pair correlation energy, $4\pi r^2 \Delta(r) \tilde{\rho}'_{nlj}(r)$ in the $N = 86$ isotones, obtained by the self-consistent Skyrme HFB theory using Green's function method for the volume pairing case.

As seen in Fig. 5(a), the neutron pair potential $\Delta(r)$ of the volume pairing is concentrated strongly within the region $r \lesssim 8$ fm, in clear contrast to the pair potential with the significant surface enhancement shown in Fig. 4(a). On the other hand, the neutron pair density $4\pi r^2 \tilde{\rho}'_{nlj}(r)$ associated with the $3p_{1/2}$ quasiparticle state, shown in Fig. 5(b), extends outside the nuclear surface $r = 7$–15 fm, and this spatial extension grows as the drip-line is approached [in a similar manner seen in Fig. 3(c), but to a slightly smaller extent]. Since the overlap of the two quantities, i.e., the product $4\pi r^2 \Delta(r) \tilde{\rho}'_{nlj}(r)$ corresponding to the integrand of the pair correlation energy, is then confined inside the surface region ($r \lesssim 8$ fm), the external part ($\gtrsim 8$ fm) of the pair density of the $3p_{1/2}$ quasiparticle state does not contribute to the pair correlation energy, leading to a small effective pairing gap. Indeed the effective pairing gaps $\Delta'_{uv,nlj}$ of the $3p_{3/2}$ and $3p_{1/2}$ states decrease from 0.558 and 0.528 MeV, respectively, in ^{136}Sn, to 0.392 and 0.370 MeV in ^{128}Mo by about 30% as approaching the drip-line. The decrease is larger than that (10–12 %) for the surface-enhanced DDDI. Taking the most weakly bound nucleus ^{128}Mo for instance, the effective pairing gaps 0.392 and 0.370 MeV of the $3p$ quasiparticle states for the volume pairing are notably smaller than the corresponding numbers 0.529 and 0.501 MeV in the case of the surface-enhanced DDDI (Table I). The smaller effective pairing gaps indicate a larger decoupling effect.

We note, however, that, the decoupling effect found in the above analysis is not as large as what is discussed in Refs. [21–24]. For the most weakly bound nucleus ^{128}Mo, the effective pairing gaps keep 62% and 58% of the total (0.635 MeV) for the unbound $3p_{3/2}$ and $3p_{1/2}$ states, respectively, still sizably larger than that suggested ($< 1/3$) in Ref. [23]. Even in the volume pairing case, the unbound $3p$ quasiparticle states persist to feel the pair potential and contribute to the pair correlation to some extent.

IV. CONCLUSIONS

We have investigated the neutron pair correlation in neutron-rich nuclei with small neutron separation energies by means of the fully self-consistent continuum Skyrme HFB theory, in which the Green's function method is utilized to describe precisely the asymptotic behavior of scattering waves for the unbound quasiparticle states in the continuum. We have clarified how weakly bound and unbound neutron orbits contribute to the pair correlation properties, especially the orbits with the low angular momentum $l = 1$ which have large spatial extensions. We have chosen the even-even $N = 86$ isotones in the Sn-Mo region for numerical analysis, and investigated, in detail, the pairing properties associated with the neutron $3p_{3/2}$ and $3p_{1/2}$ orbits, whose Hartree-Fock single-particle energies (resonances) vary in the interval of $-0.5\ \mathrm{MeV} < \varepsilon < 0.7\ \mathrm{MeV}$, covering both weakly bound and unbound cases.

We found the following features from the numerical analysis. When the $3p$ quasiparticle states are embedded in the continuum above the threshold, they immediately become broad resonances with large widths. This is because the barrier height of the Hartree-Fock plus centrifugal potential is low for the p orbits (~ 0.35 MeV in the present examples), and also because the pair potential which remains effective around the barrier region gives rise to additional coupling to the scattering wave in the exterior. The numerical results show that the width of the quasiparticle resonances of the $3p$ states are comparable to the excitation energy measured from the threshold. In spite of such a large width ($\Gamma \sim 1$ MeV), the contribution of the broad quasiparticle resonances to the pair correlation remains finite or can even increase. We found that the effective pairing gaps of the broad quasiparticle resonances have a comparable size to the total average pairing gap, indicating that the continuum quasiparticle states persist to contribute to the pair correlation. To be more precise, there exists some reduction of the effective pairing gap of $20-25$ % from the total average gap. However, this reduction of the effective pair gap is much smaller than what is discussed in Ref. [23].

Summarizing, even the broad quasiparticle p-wave resonances in the continuum do contribute to the pair correlation as long as it is located not far from the Fermi energy. This is different from the decoupling scenario [21–24]. The reason for the difference is that the pair correlation in the present study is described self-consistently using the effective pairing interaction which has enhancement outside the nuclear surface, and in this case the pair potential is enhanced largely around the surface and proximate exterior, keeping an overlap with the low-l resonant quasiparticle states.

ACKNOWLEDGMENTS

The work was partly supported by the Grant-in-Aid for Scientific Research (Nos. 20540259, 21105507, and 21340073) from the Japan Society for the Promotion of Science, the Niigata University Global Circus Program for International Student Exchanges, and also the Major State 973 Program (Grant No. 2007CB815000) as well as the National Natural Science Foundation of China (Grant Nos. 10775004 and 10975008).

[1] I. Tanihata *et al.*, Phys. Rev. Lett. **55**, 2676 (1985).
[2] G. F. Bertsch and H. Esbensen, Ann. Phys. (NY) **209**, 327 (1991); H. Esbensen and G. F. Bertsch, Nucl. Phys. A **542**, 310(1992).
[3] P. G. Hansen and B. Jonson, Europhys. Lett. **4**, 409 (1987).
[4] J. Meng and P. Ring, Phys. Rev. Lett. **77**, 3963 (1996).
[5] J. Meng and P. Ring, Phys. Rev. Lett. **80**, 460 (1998).
[6] J. Meng, H. Toki, J. Y. Zeng, S. Q. Zhang, and S.-G. Zhou, Phys. Rev. C **65**, 041302(R) (2002).
[7] S. Q. Zhang, J. Meng, and S.-G. Zhou, Sci. China Ser. G **46**, 632 (2003).
[8] M. Grasso, S. Yoshida, N. Sandulescu, and Nguyen Van Giai, Phys. Rev. C **74**, 064317 (2006).
[9] J. Terasaki, S. Q. Zhang, S. G. Zhou, and J. Meng, Phys. Rev. C **74**, 054318 (2006).
[10] V. Rotival, K. Bennaceur, and T. Duguet, Phys. Rev. C **79**, 054309 (2009).
[11] A. Bulgac, preprint FT-194-1980, Bucharest, 1980, arXiv:nucl-th/9907088v2.
[12] J. Dobaczewski, H. Flocard, and J. Treiner, Nucl. Phys. A **422**, 103 (1984).
[13] S. T. Belyaev, A. V. Smirnov, S. V. Tolokonnikov, and S. A. Fayans, Sov. J. Nucl. Phys. **45**, 783 (1987).
[14] J. Meng, Nucl. Phys. A **635**, 3 (1998).
[15] J. Dobaczewski, W. Nazarewicz, T. R. Werner, J. F. Berger, C. R. Chinn, and J. Dechargé, Phys. Rev. C **53**, 2809 (1996).
[16] M. Grasso, N. Sandulescu, N. Van Giai, and R. J. Liotta, Phys. Rev. C **64**, 064321 (2001).
[17] M. Yamagami, Phys. Rev. C **72**, 064308 (2005).
[18] H. Oba and M. Matsuo, Phys. Rev. C **80**, 024301 (2009).
[19] J. Dobaczewski, W. Nazarewicz, and P.-G. Reinhard, Nucl. Phys. A **693**, 361 (2001).
[20] M. Matsuo, K. Mizuyama, and Y. Serizawa, Phys. Rev. C **71**, 064326 (2005).
[21] I. Hamamoto and B. R. Mottelson, Phys. Rev. C **68**, 034312 (2003).
[22] I. Hamamoto and B. R. Mottelson, Phys. Rev. C **69**, 064302 (2004).
[23] I. Hamamoto, Phys. Rev. C **71**, 037302 (2005).
[24] I. Hamamoto, Phys. Rev. C **73**, 044317 (2006).

[25] S. A. Fayans, S. V. Tolokonninkov, and D. Zawischa, Phys. Lett. B **491**, 245 (2000).
[26] J. Meng, H. Toki, S.-G. Zhou, S. Q. Zhang, W. H. Long, and L. S. Geng, Prog. Part. Nucl. Phys. **57**, 470 (2006).
[27] S.-G. Zhou, J. Meng, and P. Ring, Phys. Rev. C **68**, 034323 (2003).
[28] S.-G. Zhou, J. Meng, P. Ring, and E.-G. Zhao, Phys. Rev. C **82**, 011301(R) (2010).
[29] W. H. Long, P. Ring, N. Van Giai, and J. Meng, Phys. Rev. C **81**, 024308 (2010).
[30] K. Bennaceur, J. Dobaczewski, and M. Ploszajczak, Phys. Lett. B **496**, 154 (2000).
[31] Y. M. Engel, D. M. Brink, K. Goeke, S. J. Krieger, and D. Vautherin, Nucl. Phys. A **249**, 215 (1975).
[32] M. Bender, P.-H. Heenen, and P.-G. Reinhard, Rev. Mod. Phys. **75**, 121 (2003).
[33] J. Meng, Phys. Rev. C **57**, 1229 (1998).
[34] M. Matsuo, Nucl. Phys. A **696**, 371 (2001); Prog. Theor. Phys. Suppl. **146**, 110 (2002).
[35] E. Chabanat, R. Bonche, R. Haensel, J. Meyer, and R. Schaeffer, Nucl. Phys. A **635**, 231 (1998).
[36] M. Matsuo, Y. Serizawa, and K. Mizuyama, Nucl. Phys. A **788**, 307c (2007).
[37] M. Matsuo, Phys. Rev. C **73**, 044309 (2006).
[38] M. Matsuo and Y. Serizawa, Phys. Rev. C **82**, 024318 (2010).